Spin-density-wave transition of Fe1 zigzag chains and metamagnetic transition of Fe2 in TaFe_{1+y}Te_{3}

R. H. Liu, M. Zhang, P. Cheng, Y. J. Yan, Z. J. Xiang, J. J. Ying, X. F. Wang, A. F. Wang, G. J. Ye, X. G. Luo, and X. H. Chen

Phys. Rev. B **84**, 184432 — Published 28 November 2011

DOI: 10.1103/PhysRevB.84.184432

Spin density wave transition of Fe1 zigzag chains and metamagnetic transition of Fe2 in $TaFe_{1+y}Te_3$

R. H. Liu, M. Zhang, P. Cheng, Y. J. Yan, Z. J. Xiang, J. J. Ying,
X. F. Wang, A. F. Wang, G. J. Ye, X. G. Luo and X. H. Chen*
Hefei National Laboratory for Physical Science at Microscale and Department of Physics, University of Science and Technology of China, Hefei, Anhui 230026, People's Republic of China

The mixed-metal-network layered compound $TaFe_{1+y}Te_3$ with a "sandwich" $TaFeTe_3$ layer has partial iron atoms Fe2 randomly occupying these interstitial sites of tetrahedral (Ta, Fe)Te, similar to that in iron-based high-T_c superconductor $Fe_{1+y}Te$. The antiferromagnetic (AFM) transition of Fe1 zigzag chains and spin-flop of these interstitial Fe2 under high magnetic field are studied through susceptibility, magnetoresistance (MR), Hall effect and specific heat measurements in high-quality single crystal $TaFe_{1+y}Te_3$. These properties suggest that the high temperature AFM transition of the $TaFeTe_3$ layers should be a spin-density-wave type AFM order. Below T_N, the spin-flop of these interstitial Fe2 from antiferromagnetism to ferromagnetism induces an sharp drop on resistivity and an anomalous Hall effect. It can be inferred from the spin-flop of Fe2 that the local moment of Fe2 atom is about 4 μ_B/Fe. The possible magnetic structure of $TaFe_{1+y}Te_3$ is proposed from the susceptibility, MR and Hall effect. The properties related to the spin-flop of Fe2 supply a good opportunity to study the coupling between Fe1 and Fe2 in these $TaFe_{1+y}Te_3$ or $Fe_{1+y}Te$ compounds with interstitial Fe2.

PACS numbers: 75.50.Ee, 75.30.Gw, 75.30.Kz, 74.70.Xa

I. INTRODUCTION

The discovery of iron-based high temperature superconductors has generated great interests in exploring layered Fe-based pnictides and chalcogenides[1–4]. The superconducting transition temperature (T_c) in iron chalcogenides α-FeSe increased from initial 8 K[4] to 15 K by partial Te substitution for Se[5,6], and up to 37 K under high pressure[7,8]. Recently, the new intercalated iron selenides $A_xFe_{2-y}Se_2$ (A = K, Rb, Cs and Tl)[9–12] were reported to have T_c around 32 K, even 43 K. Although the presently known maximum critical temperatures are lower than that of the iron pnictides, these iron chalcogenides have attracted considerable attention due to the fact that it is virulent As free, and that they have very interesting coexistence and competition relation between magnetism and superconductivity[13,14]. The observation of spin resonance below T_c and enhancement of spin fluctuation near T_c in iron chalcogenides suggest a superconducting pairing mechanism mediated by spin fluctuation. The high pressure and muon spin rotation (μSR) experiments indicate the static magnetic phase microscopically coexists with superconductivity in $FeSe_{1-x}$ under pressure. In addition, the magnetic order temperature (T_N) and superconducting transition temperature (T_c) are both enhanced by pressure[13,14]. In the intercalated iron selenides, μSR[15,17], neutron scattering[16] and high temperature magnetization and resistivity[18] also indicate that superconductivity coexists with antiferromagnetism (AFM) with high T_N (T_N = 470 - 550 K) and large magnetic moment 2-3.3 μ_B/Fe[16,17]. Furthermore, $Fe_{1+y}Te$ has the most simple crystal structure in iron based superconductors. It is stacked with anti-PbO-type FeTe layer along c-axis, in which iron atoms (Fe1) form a square plane in the edge-sharing FeTe tetrahedral layer. $Fe_{1+y}Te$ always contains excess iron atoms (Fe2), which randomly occupy the interstitial sites of FeTe layer and directly couple with the four nearest neighbor Fe1 atoms in the iron square plane[19,20]. This structural characteristic is analogous to that of PbFCl-type Fe_2As, where one half iron atoms (Fe1) and As form edge-sharing tetrahedral network, and the other half of iron atoms (Fe2) fully occupy these interstitial sites between anti-PbO type FeAs layers. Fe_2As compound also has a spin-density-wave (SDW) type AFM order at 353 K[21], which is higher than T_N in FeAs-based parent compounds.

The $Fe_{1+y}Te$ is not superconducting until Te atoms are partially replaced by Se or S and excess iron atoms (Fe2) are also removed simultaneously[5,6]. Similar to iron-pnictides, $Fe_{1+y}Te$ exhibits a structural and AFM transition simultaneously near $T_N \sim$ 60 - 70 K. The different T_N arise from the different contents of excess partial iron atoms (Fe2)[4–6,19,20]. However, its AFM structure is distinct from that in FeAs-based parent compounds. A collinear commensurate AFM order with Fe moment along a-axis has been identified in the iron-pnictides[22,31], while $Fe_{1+y}Te$ has a bicollinear and 45^o rotated AFM order[24,25]. In addition, neutron scattering experiment found that interstitial Fe2 could tune the AFM wave vector from commensurate to incommensurate in $Fe_{1+y}Te$ when y is increased to above 0.076. Theory suggests that the interstitial Fe2 with a valence near Fe^+ donates charge to the FeTe layers[26]. There is also a very strong tendency toward moment formation on the Fe2, then these interstitial Fe2 with a large local moment will interact with the magnetism of the FeTe layers, complicating the magnetic order[24–27]. Here we report a mixed-metal-network layered compound $TaFe_{1+y}Te_3$, which has also partial iron atoms Fe2 randomly occupying these interstitial sites of tetrahedral (Ta,Fe)Te[28–30], similar to

that in $Fe_{1+y}Te$. $TaFe_{1+y}Te_3$ has a SDW-type AFM order (T_N) at 160 - 200 K depending on the contents of interstitial Fe2 atoms. In addition, below T_N, these Fe2 atoms directly couple with the three nearest Fe1 atoms of Ta-Fe1 mixed network layers and also form AFM alignment, but external magnetic field ($\mathbf{H}_{ext}$) is able to break the coupling between Fe1 and Fe2, and cause Fe2 to take a spin-flop and form ferromagnetic (FM) alignment from AFM alignment. It offers an interesting opportunity to investigate the interplay between excess Fe2 and magnetism and transport properties of Ta-Fe mixed network layer.

II. EXPERIMENTAL DETAILS

Single crystals of $TaFe_{1+y}Te_3$ were grown by chemical vapor transport method[28,29]. Ta (3N) powder, Fe (3N) powder and Te (4N) powder were accurately weighed according to the stoichiometric ratio of $TaFe_{1+y}Te_3$ (y = 0 - 0.25), then thoroughly grounded and pressed into pellets. The 2 g mixture pellets and 30 mg transport agent $TeCl_4$ were sealed in evacuated 18 cm long × 15 mm diameter quartz tube. The sealed tubes were placed in multi-zones tube furnace and slowly heated to temperature with the hot end at 690 °C and the cool end at 630 °C. After 150 hours, the furnace was shut off and cooled down to room temperature. The long narrow crystals were obtained, but in different temperature zones the samples had different contents of interstitial Fe2. The sample preparation process except for annealing was carried out in glove box in which high pure argon atmosphere is filled. Single crystal X-ray diffraction (XRD) was performed by MAC MXPAHF X-ray diffractometer (Japan) at room temperature. Elemental analysis obtained by Energy Dispersive X-ray Spectroscopy (EDX). Magnetic susceptibility measurement was performed by a SQUID magnetometer (Quantum Design MPMS-XL7s). Magnetoresistance (MR), Hall coefficient (R_H), heat capacity and thermoelectric power (TEP) were measured by using Quantum Design PPMS.

III. RESULTS AND DISCUSSION

A. Crystal structure

The structure of $TaFe_{1+y}Te_3$ is shown in the right inset of Fig. 1a. The structure of $TaFe_{1+y}Te_3$ features a Ta-Fe bonded network, and the mixed metal network lies between tellurium layers, forming a $FeTaTe_3$ "sandwich"[28,29,31], similar to that of anti-PbO type FeTe layer. It is stacked with $FeTaTe_3$ "sandwich" along ($-l$ 0 l), and crystallizes in $P2_1/m$ monoclinic symmetry with lattice constants $a = 7.4262$ Å, $b = 3.6374$ Å, $c = 9.9925$ Åand $\beta = 109.166$ °. According to literatures[28,30], there are always partial excess iron atoms, which randomly occupy the interstitial sites of $FeTaTe_3$ layers[30], similar to

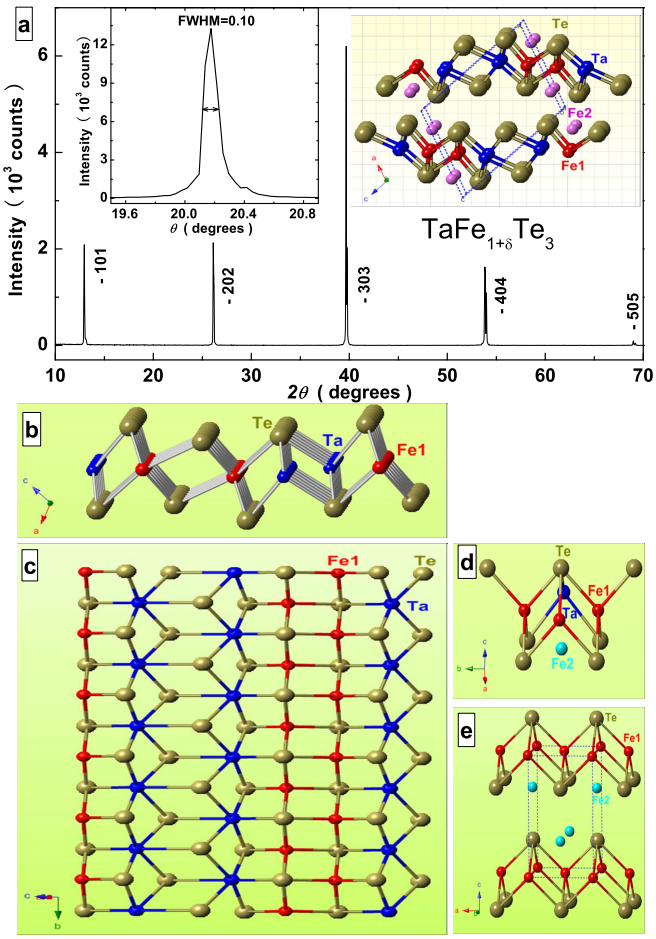

FIG. 1: (a) The single crystal X-ray diffraction pattern for $TaFe_{1+y}Te_3$. The left inset shows the rocking curve at the (-3 0 3) reflection. The crystal structure is shown in the right inset; (b) A view of the $TaFeTe_3$ "sandwiched" structure along b-axis. There are two unique zigzag chains that are parallel to the b-axis; (c) A view of the mixed metal network $TaFeTe_3$ along ($-l$ 0 l); (d) The zigzag chain is made up of Fe centered edge-sharing tetrahedra, similar to the $FeTe_4$ tetrahedra of anti-PbO type $Fe_{1+y}Te$. The partial Fe2 atoms randomly occupy the interstitial sites of the (Ta,Fe)Te layers; (E) The structure of anti-PbO type $Fe_{1+y}Te$. The partial Fe2 atoms also randomly occupy the interstitial sites of anti-PbO type FeTe layers.

that in $Fe_{1+y}Te$. Fig. 1a shows XRD pattern of the platelet-shaped $TaFe_{1+y}Te_3$ single crystal at room temperature. Only ($-l$ 0 l) reflections are observed in XRD pattern, indicating that the $FeTaTe_3$ "sandwich" plane parallels to the surface of the long piece-like single crystal. The full width of half maximum (FWHM) in the rocking curve of the (-3 0 3) reflection is 0.1 °, shown as the left inset of Fig. 1a, suggesting it is a high quality single crystal. A view of the $FeTaTe_3$ "sandwich" structure along b-axis is shown in Fig. 1b. There are two unique zigzag chains that are parallel to the b-axis. The view nearly perpendicular to the Ta-Fe mixed network layer is

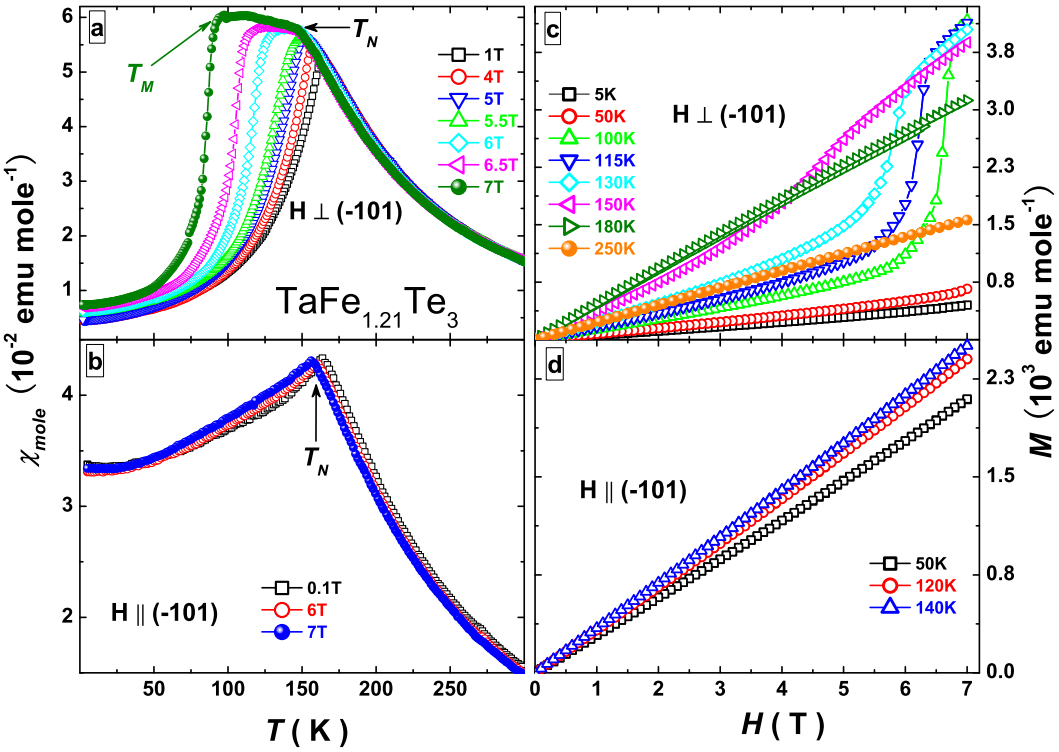

FIG. 2: Temperature dependence of susceptibility measured under different fields perpendicular to sample plane (a) or along sample plane (b). Field dependence of magnetization **M** at various temperature with field perpendicular to sample plane (c) or along sample plane (d).

shown in Fig. 1c. One can easily see that one chain consists of Ta-centered octahedra which shares Te-Ta edges. The other chain is made up of Fe-centered edge-sharing tetrahedra. These two zigzag chains alternately build up the Ta-Fe mixed networks. From another point of view, the Ta-Fe mixed metal $FeTaTe_3$ layer is made up of (Ta,Fe)Te tetrahedra Ta-Fe-Fe-Ta ribbons contacted by sharing-edge Te-Te. The coordination environment of Fe1 in the $FeTaTe_3$ "sandwich" layer is the same as that of $FeTe_4$ tetrahedra in anti-PbO type FeTe layer. Additionally, there are partial excess Fe2 atoms occupying randomly in square pyramidal sites formed by five Te atoms. The (Ta,Fe)Te_4 tetrahedra structure of $FeTaTe_3$ "sandwich" layer and $Fe_{1+y}Te$ structure are shown in Fig. 1d and Fig. 1e, respectively.

B. Magnetic susceptibility and magnetoresistance

Temperature dependence of susceptibility under different magnetic fields perpendicular and parallel to the plane of single crystal are shown in Fig. 2a and Fig. 2b, respectively. From the single crystal XRD pattern, we know that the Ta-Fe mixed metal network is parallel to the plane of single crystal. The susceptibility under low field shows a sharp antiferromagnetic transition at $T_N \sim 160$ K, which is lower than $T_N = 200$ K of polycrystalline sample $TaFe_{1.25}Te_3$. Elemental analysis of the single crystal with $T_N = 160$ K obtained by EDX indicates that interstitial iron is about 0.21. This suggests that interstitial iron atoms Fe2 have strong effect on the magnetism of the Fe zigzag chains. Less excess iron will result in lower T_N. When external magnetic field is perpendicular to the Ta-Fe mixed metal network, the AFM order temperature T_N is weakly suppressed from $T_N = 160$ K at 0.1 T to $T_N = 150$ K at 7 T, and the more interesting thing is that high field induces ferromagnetic behavior in susceptibility below T_N. Below T_N susceptibility firstly keeps constant with temperature decreasing, then sharply drops at certain temperature T_M, which depends on the value of external field H. At 160 K Fe1 of zigzag chains form AFM order, and also induce that excess Fe2 of interstitial sites to form antiferromagnetic order simultaneously due to the direct coupling of Fe1 and Fe2. Below T_N magnetic moment of excess Fe2 tends to align along the direction of external field H, and forms ferromagnetic order due to the coupling of Fe2 and external field. This is the reason why susceptibility keeps a constant under higher vertical magnetic field below T_N. The external field $\mathbf{H}_{ext}$ and the inner field $\mathbf{H}_{int}$ formed by Fe1 zigzag chains have a competition in tuning direction of magnetic moment of Fe2 below T_N. The external field

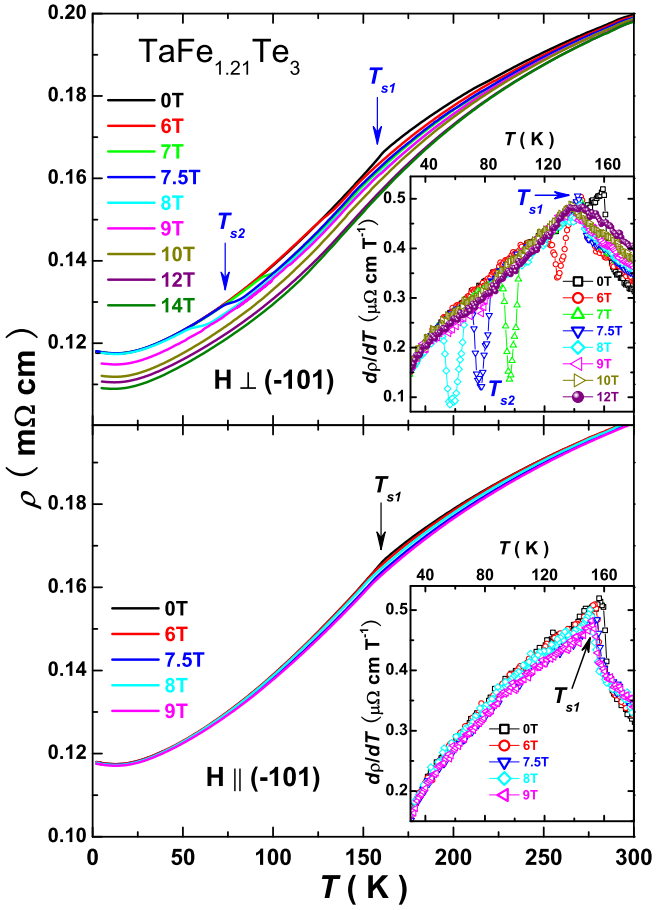

FIG. 3: Temperature dependence of resistivity under different fields perpendicular to sample plane (up panel) or along sample plane (down panel). Inset: Temperature dependence of their derivative resistivity dρ/dT.

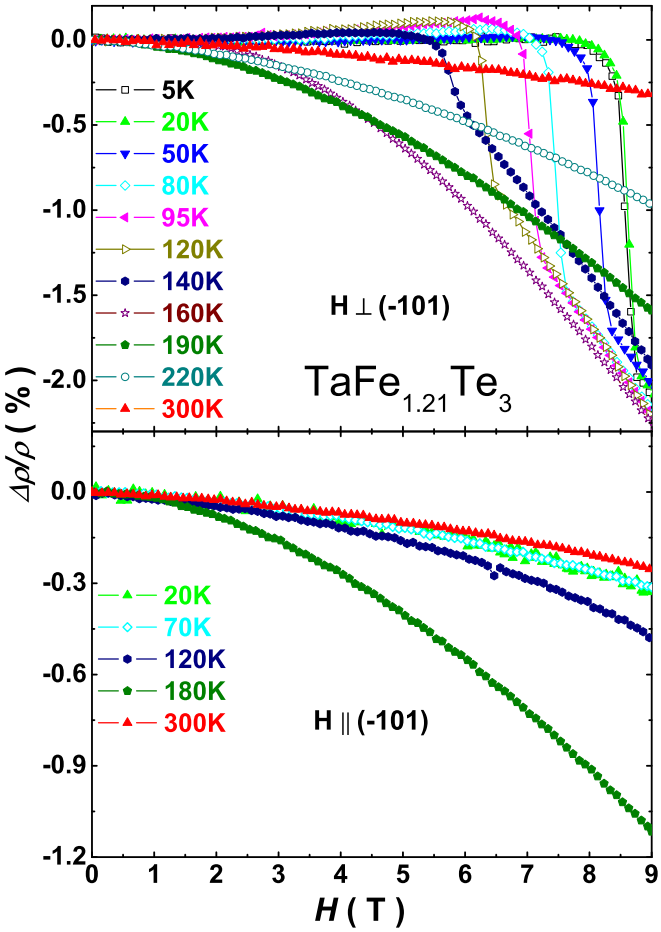

FIG. 4: Isothermal magnetoresistance at different temperatures with field perpendicular to sample plane (up panel) or along sample plane (down panel).

is in the ascendant in tuning Fe2 to form FM alignment at high temperature, while the inner field will be in the ascendant with temperature decreasing further, which also induces the susceptibility to drop sharply at certain temperature. The susceptibility of single crystal has strong anisotropic magnetic properties at low field below T_N, suggesting that the magnetic easy axis of Fe1 zigzag is along the $[-l\ 0\ l]$. Fig. 2c and 2d show field dependence of magnetization $\mathbf{M}$ at various temperature with field perpendicular and parallel to Ta-Fe mixed network, respectively. When external magnetic field is perpendicular to Fe1 zigzag of Ta-Fe mixed network, magnetization $\mathbf{M}$ increases linearly with the external field $\mathbf{H}_{ext}$ at low field and shows sharp ferromagnetic-like transition at certain field H_C. But the magnetic hysteresis is not observed in ***M-H*** curves at Fig. 2c and 2d. It also arises from the result that the external field $\mathbf{H}_{ext}$ competes with the inner field $\mathbf{H}_{int}$ formed by Fe1 zigzag chains for tuning the direction of Fe2 spin.

Figure 3 shows temperature dependence of resistivity in various magnetic field $\mathbf{H}$. The resistivity shows a metal behavior and has an abnormal transition at $T_{S1} \sim 160$ K under low field, corresponding to the drop of magnetic susceptibility. When external magnetic field is parallel to the Ta-Fe mixed metal network, the abnormal transition temperature T_{S1} has almost no change at different fields. However, under high field perpendicular to the single crystal plane T_{S1} is weakly suppressed to low temperature ($T_{S1} = 150$ K for $\mathbf{H} > 6$ T) and the resistivity has another abnormal transition simultaneously at certain low temperature T_{S2}, which depends on the magnitude of external field $\mathbf{H}$. These abnormal behaviors of resistivity can be easily seen in these inters of Fig. 3. The T_{S1} and T_{S2} in resistivity correspond with the AFM transition temperature T_N of Fe1 and the metamagnetic transition temperature T_M of Fe2 in magnetic susceptibility, respectively.

To confirm the origin of the anomalous in resistivity, isothermal magnetoresistance (MR) at different temperature is shown in Fig. 4. One can easily see that they have negative MR effect under parallel field for all temperature and under vertical field for higher than T_N. For

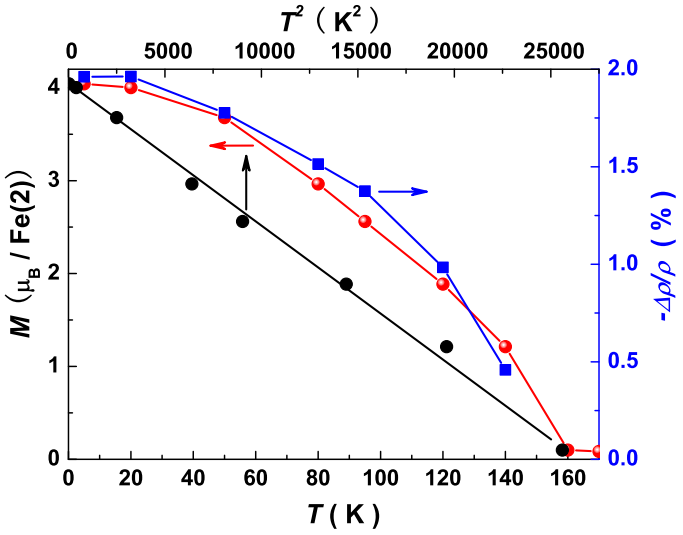

FIG. 5: Magnetization of Fe2 $\boldsymbol{M}$ vs T (Left Y-axis) and magnetoresistance $\Delta\rho(T)/\rho(T)$ vs T (Right Y-axis). $\boldsymbol{M}$ vs T^2 (Up X-axis) shows $\Delta M(T)/M(0) \propto T^2$ up to 160 K.

vertical field, they have small positive MR below the certain field H_C, and it shows a sharp negative MR around H_C, which should be ascribed to spin-flop of Fe2 at certain field H_C. The largest negative MR effect appearing at a little higher temperature than T_N suggests that there is strong magnetic fluctuation around T_N. The temperature dependence of normal Hall coefficient R_H also supports this point of view.

Figure 5 shows the "spontaneous" magnetization $\mathbf{M}$ of Fe2, which is inferred from the jump magnitudes ΔM in the isothermal magnetization. The saturation magnetization at 5 K is 4 ± 0.2 μ_B per Fe2, which is the same with local moment Fe (4 μ_B/Fe) in $Fe_{1/4}TaS_2$. The transition metal intercalated dichalcogenide $Fe_{1/4}TaS_2$ has a ferromagnetic transition at $T_C \sim 160$ K, in which the spontaneous magnetization of Fe is strongly pinned perpendicular to the TaS_2 layers by a very large anisotropy field below T_C[33]. Neutron scattering experiments reveal that the Fe has a total moment 2.25(8) μ_B/Fe in $Fe_{1+y}Te$[25]. Since the moments of the partial Fe2 ions are randomly distributed in the interstitial sites of FeTe layers, it is difficult to estimate the moment sizes of excess Fe2 by using conventional neutron diffraction[24,25]. However, the theoretical calculation suggests that the excess Fe2 has very strong magnetism with high local moment[26]. We find that magnetization of excess Fe2 has a near perfect T^2 dependence below T_N, in agreement with normal ferromagnetic metals[34], as shown in Fig. 5. The spin-flop of Fe2 tuned by field induces a sharp negative MR ($\Delta\rho(T)/\rho(T)$) around H_C, as shown in Fig. 5. $\Delta\rho(T)/\rho(T)$ and magnetization $\mathbf{M}$ of Fe2 have the same dependence of temperature. $\frac{\Delta\rho/\rho}{M_{Fe2}}$ is about 0.45 % perμ_B(Fe2). We use the Curie-Weiss expression $\chi = \chi_o + C/(T+\Theta)$ to fit the susceptibility data from 330 to 400 K, where C is the Curie constant, Θ the Weiss temperature and χ_o constant. The total effective moment of 3.9 μ_B per iron atom is obtained from the Curie constant. It is a little larger than the result 3.7 μ_B in previous literature, in which the susceptibility of polycrystalline sample is fitted by the Curie-Weiss expression from 450 to 1000 K[28]. From MR and the following Hall coefficient result, we know that there is very strong magnetic fluctuation or magnetic correlation between iron atoms above T_N. The temperature range of susceptibility fitted from 330 to 400 K is too low and brings some deviation of total effective moment inferred. In spite of the small deviation, the magnetic moment of the Fe1 (3.7 ±0.2 μ_B) in Ta-Fe-Fe-Ta ribbons of the $TaFeTe_3$ "sandwich" is almost two times larger than that of Fe1 (2.25 μ_B) in the anti-PbO type FeTe layers.

C. Hall coefficient and thermoelectric powder

It is well known that Hall effect arises from two parts-normal Hall effect and anomalous Hall effect in ferromagnetic metals, in which anomalous Hall resistivity is proportional to the magnetization $\mathbf{M}$. Empirically, one finds Hall resistivity $\rho_H = \rho_{OH} + \rho_{AH} = R_H^N + R_H^A 4\pi M$, where ρ_{OH} is the normal Hall resistivity due to the Lorentz force in a perpendicular magnetic field $\mathbf{B}$, ρ_{AH} the anomalous Hall resistivity, R_H^N the normal Hall coefficient, and R_H^A the anomalous Hall coefficient[32]. To confirm the origin of the AFM transition of Fe1 zigzag chains and field inducing FM transition of Fe2, the transverse resistivity ρ_{xy} is measured by sweeping field from -9 T to +9 T at various temperature, and the accurate Hall resistivity ρ_H is obtained, as shown in Fig. 6a, by using $[\rho_{xy}(+H) - \rho_{xy}(-H)]/2$, where $\rho_{xy}(\pm H)$ is ρ_{xy} under positive or negative magnetic field. Similar to the isothermal MR at various temperature, ρ_H also shows a steep rise at certain field H_C below T_N, which arises from the jump magnitudes of magnetization $\mathbf{M}$ due to the spin-flop of excess Fe2 induced by external field $\mathbf{H}$. The normal Hall coefficient R_H^N is obtained from these H-linear term of ρ_H below the "coercive" field H_C. R_H^N dependence of temperature is shown in Fig. 5. The R_H^N is positive, indicating the carrier is hole. Above T_N, R_H^N decreases distinctly with temperature increasing and almost has a linear dependence of temperature. It may arise from the strong magnetic fluctuation above T_N in this system. Empirically, the change of R_H^N is weakly dependent on temperature above T_C in general ferromagnetic metal. R_H^N shows a pronounced dip at T_N. It should be ascribed to that the magnetic fluctuation is suppressed completely and the transport lifetime τ has a strong change around the fermi surface below T_N. The Hall number density $n_H = 1/eR_H^N$ varies from the minimal value 1.3×10^{21} cm^{-3} at 155 K to 1.4 $\times10^{22}$ cm^{-3} at 75 K. The normal Hall coefficient R_H^N is the same to that of $Fe_{1+y}Te$($R_H \sim 10^{-9} m^3/C$)[27]. The thermoelectric power (TEP) is positive and has the same sign of the Hall coefficient. As shown in Fig. 6b, TEP shows a weak temperature depen-

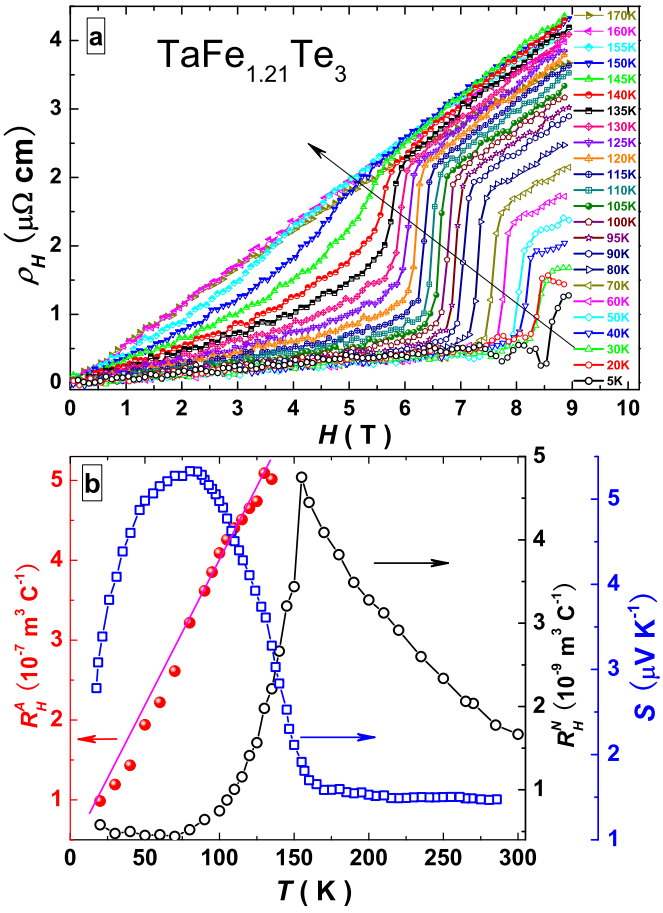

FIG. 6: (a) Field dependent Hall resistivity ρ_H at various temperatures are obtained by using $[\rho_{xy}(+H) - \rho_{xy}(-H)]/2$, where $\rho_{xy}(\pm H)$ is ρ_{xy} under positive or negative magnetic field. (b) The temperature dependence of anomalous Hall coefficient R_H^A, normal Hall coefficient R_H^N and thermoelectric power S. R_H^A is inferred from the jump in ρ_H at "coercive" field H_C, while R_H^N is inferred from the H-linear portions of ρ_H below H_C.

dence above $T_N \sim 160$ K, but it has a pronounced rise below T_N and arrives at the maximum (5.2 μV/K) around 75 K. The resistivity, susceptibility, R_H^N and TEP show anomalous behaviors below T_N, which are very similar to that in metal Cr around SDW-type AFM transition[35]. In addition, the structure of $TaFe_{1+y}Te_3$ features a Fe1 zigzag chains along b-axis. It is well known that many low dimensional materials have SDW and charge density wave (CDW) instability at low temperature[36,37]. The behaviors of these physical properties at T_N suggest that the transition should be a SDW-type AFM transition. The anomalous Hall coefficient R_S^A below T_N is inferred from the ratio of the jump magnitudes ΔM and $\delta\rho_H$ around H_C. $R_S^A = \Delta\rho_H/4\pi M$ is also plotted in Fig .6b. R_S^A decreases linearly with temperature below T_N.

D. Heat capacity

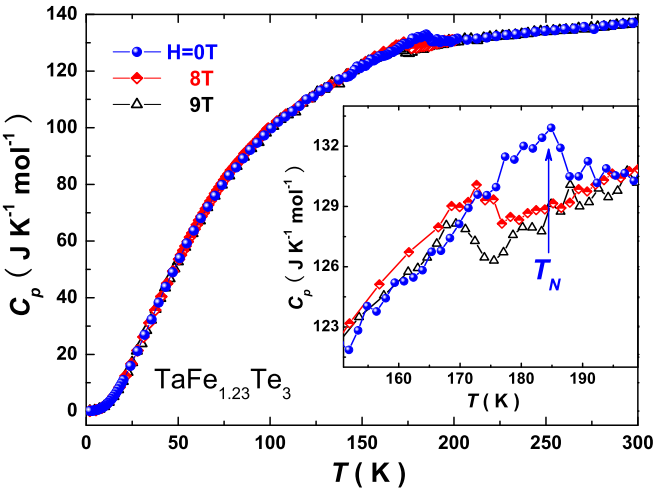

FIG. 7: Temperature dependence of specific heat for $TaFe_{1.23}Te_3$ under different fields perpendicular to sample plane.

In order to confirm the AFM transition, the heat capacity was measured by a relaxation-time method with a Quantum Design PPMS. One can clearly see a pronounced anomaly peak of $C_p(T)$ at 185 K for zero field in Fig.7. The temperature is different from the T_N inferred by susceptibility due to different samples with different magnitude of excess Fe. The sample measured specific heat has 0.23 interstitial Fe2 confirmed by EDX. The temperature of specific heat peak is shifted from 185 K to 170 K at 9 T in excellent agreement with the previous susceptibility and MR under high field. They consistently confirm that high magnetic field suppress the AFM order of Fe1 zigzag chains distinctly. In the low-temperature region the specific heat is of the form $C_p = \gamma T + \beta T^3$. The Debye temperature can be estimated from the equation $\beta = (12\pi^4 N k_B)/(5\Theta_D^3)$, where N is the number of atoms per formula unit. From the plot of C_p/T vs.T^2 data between 2 and 14 K, we can estimate a Sommerfeld coefficient $\gamma = 25.86$ mJ K^{-2} mol^{-1}, $\beta = 1.496$ mJ K^{-4} mol^{-1} and $\Theta_D = 189$ K for $TaFe_{1.23}Te_3$. The electron specific heat coefficient γ is close to that of $Fe_{1+y}Te$ (γ=27 mJ K^{-2} mol^{-1})[27]. The above resistivity and normal Hall coefficient R_H^N also show that $Fe_{1+y}Te$ and $TaFe_{1+y}Te_3$ have the same order of magnitude. It suggests that $Fe_{1+y}Te$ and $TaFe_{1+y}Te_3$ have almost the same density of states near the Fermi energy level.

E. Models of magnetic structure

Based on the above results of susceptibility, MR and Hall effect, possible magnetic structures for the spins of Fe1 and Fe2 are proposed shown in Fig. 8a and 8b. Be-

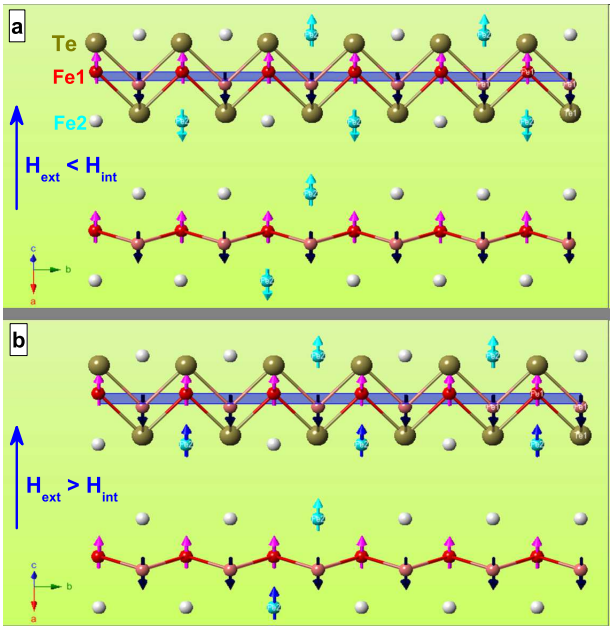

FIG. 8: The spin model of excess Fe and Fe zigzag chain with external magnetic field **H** along $(-l\ 0\ l)$: (a) $0 \leq \mathbf{H}_{ext} < \mathbf{H}_{int}$; (b) $\mathbf{H}_{ext} > \mathbf{H}_{int}$.

low T_N, Fe1 atoms of zigzag chains form antiferromagnetic alignment. The magnetic easy axis of Fe1 should be perpendicular to the Ta-Fe mixed metal network layers with a very large anisotropy energy. Since excess Fe2 directly couples with Fe1 of zigzag chains, the random excess Fe2 forms ferromagnetic alignment with nearest two Fe1 due to the inner field $\mathbf{H}_{int}$ induced by Fe1 in zigzag chain below T_N. Furthermore, the inner field and the coupling energy between Fe2 and Fe1 are both enhanced with temperature decreasing. On the other hand, the external field $\mathbf{H}_{ext}$ has very weak suppression on the AFM transition of Fe1 in zigzag chains, but strongly tunes the direction of Fe2 spin as long as $\mathbf{H}_{ext} > \mathbf{H}_{int}$. Since the especial crystal structure and magnetic structure shown in Fig. 8, the inner field will induce the excess Fe2 up and down among Fe1 zigzag chains to form AFM alignment between Fe2(up) and Fe2(down). That is why the whole Fe form AFM alignment below T_N under low field. However, the external field prefers the all excess Fe2 to be parallel with each other along external field. When the external field overcomes the inner field with temperature increasing, it will tune Fe2 atoms which are antiparallel to external field to reverse their spins. This causes the fact that susceptibility sharply increases at the certain temperature T_M or certain field H_C, as shown in Fig. 2.

IV. CONCLUSION

In summary, we systematically study the AFM order of Fe1 zigzag chains and spin-flop of excess Fe2 under high magnetic field **H** through the susceptibility, MR, Hall effect and specific heat measurements in high-quality single crystal $TaFe_{1+y}Te_3$. These properties suggest that the high temperature AFM transition of the $TaFeTe_3$ layers should be a SDW-type AFM order. Below T_N, Fe1 antiferromangetic chains will induce a inner magnetic field $\mathbf{H}_{int}$ to excess Fe2 and lead Fe2 to form an AFM alignment, in which the magnetic coupling strength between Fe1 and Fe2 is enhanced by decreasing temperature. On the other hand, the external magnetic field $\mathbf{H}_{ext}$ competes with the inner magnetic field $\mathbf{H}_{int}$ induced by AFM order of Fe1 zigzag chains and inclines to tune excess Fe2 to form FM alignment along $\mathbf{H}_{ext}$. The excess Fe2 has a spin-flop at the "coercive" field H_C, where $\mathbf{H}_{ext}$ can overcome the $\mathbf{H}_{int}$. Based on spin-flop of Fe2, the local moment of Fe2(4 μ_B/Fe) can be obtained from $\Delta \boldsymbol{M}$ around "coercive" field H_C in **M**-**H** curves. The possible magnetic structure of $TaFe_{1+y}Te_3$ is also proposed. The properties related to the spin-flop of Fe2 supply a good opportunity to study the coupling between Fe1 and Fe2 in these $TaFe_{1+y}Te_3$ or $Fe_{1+y}Te$ compounds with excess Fe2.

ACKNOWLEDGMENT: This work is supported by the Natural Science Foundation of China and by the Ministry of Science and Technology of China (973 project No:2006CB601001) and by Natural Basic Research Program of China (2006CB922005).

* Corresponding author; Electronic address: chenxh@ustc.edu.cn

[1] Y. Kamihara, T. Watanabe, M. Hirano, and H. Hosono, J. Am. Chem. Soc. **130**, 3296 (2008).

[2] X. H. Chen, T. Wu, G. Wu, R. H. Liu, H. Chen, and D. F. Fang, Nature **354**, 761-762(2008).

[3] Z. A. Ren, G. C. Che, X. L. Dong, J. Yang, W. Lu, W. Yi, X. L. Shen, Z. C. Li, L. L. Sun, F. Zhou, and Z. X. Zhao, Europhys. Lett. **83**, 17002(2008).

[4] F. C. Hsu, J. Y. Luo, K. W. Yeh, T. K. Chen, T. W. Huang, P. M. Wu, Y. C. Lee, Y. L. Huang, Y. Y. Chu, D. C. Yan, and M. K. Wu, Proc. Natl. Acad. Sci. U.S.A. **105**, 14262(2008).

[5] K. W. Yeh, T. W. Huang, Y. L. Huang, T. K. Chen, F. C. Hsu, P. M. Wu, Y. C. Lee, Y. Y. Chu, C. L. Chen, J. Y. Luo, D. C. Yan, and M. K. Wu, Europhys. Lett. **84**, 37002(2008).

[6] M. H. Fang, H. M. Pham, B. Qian, T. J. Liu, E. K. Vehstedt, Y. Liu, L. Spinu, and Z. Q. Mao, Phys. Rev. B **78**, 224503(2008).

[7] Y. Mizuguchi, F. Tomioka, S. Tsuda, T. Yamaguchi, and Y. Takano, Appl. Phys. Lett. **93**, 152505(2008).

[8] S. Medvedev, T. M. McQueen, I. A. Troyan, T. Palasyuk, M. I. Eremets, R. J. Cava, S. Naghavi, F. Casper, V. Ksenofontov, G. Wortmann, and C. Felser, Nature materials **8**, 630(2009).

[9] J. Guo, S. Jin, G. Wang, S. Wang, K. Zhu, T. Zhou, M. He, and X. Chen, Phys. Rev. B **82**, 180520 (2010).

[10] M. H. Fang, H. D. Wang, C. H. Dong, Z. J. Li, C. M. Feng, J. Chen, and H. Q. Yuan, Europhys. Lett. **94**, 27009(2011) .

[11] Y. Mizuguchi, H. Takeya, Y. Kawasaki, T. Ozaki, S. Tsuda, T. Yamaguchi, and Y. Takano, Appl. Phys. Lett. **98**, 042511 (2011).

[12] A. F. Wang, J. J. Ying, Y. J. Yan, R. H. Liu, X. G. Luo, Z. Y. Li, X. F. Wang, M. Zhang, G. J. Ye, P. Cheng, Z. J. Xiang, and X. H. Chen, Phys. Rev. B **83**, 060512(R)(2011).

[13] M. Bendele, A. Amato, K. Conder, M. Elender, H. Keller, H. H. Klauss, H. Luetkens, E. Pomjakushina, A. Raselli, and R. Khasanov, Phys. Rev. Lett. **104**, 087003(2010).

[14] S. Margadonna, Y. Takabayashi, Y. Ohishi, Y. Mizuguchi, Y. Takano, T. Kagayama, T. Nakagawa, M. Takata, and K. Prassides, Phys. Rev. B **80**, 064506(2009).

[15] Z. Shermadini, A. Krzton-Maziopa, M. Bendele, R. Khasanov, H. Luetkens, K. Conder, E. Pomjakushina, S. Weyeneth, V. Pomjakushin, O. Bossen, and A. Amato, Phys. Rev. Lett. **106**, 117602(2011).

[16] W. Bao, Q. Huang, G. F. Chen, M. A. Green, D. M. Wang, J. B. He, X. Q. Wang, and Y. Qiu, Chin. Phys. Lett. **28**, 086104(2011).

[17] V. Yu. Pomjakushin, D. V. Sheptyakov, E. V. Pomjakushina, A. Krzton-Maziopa, K. Conder, D. Chernyshov, V. Svitlyk, and Z. Shermadini, Phys. Rev. B **83**, 144410(2011).

[18] R. H. Liu, X. G. Luo, M. Zhang, A. F. Wang, J. J. Ying, X. F. Wang, Y. J. Yan, Z. J. Xiang, P. Cheng, G. J. Ye, Z. Y. Li, and X. H. Chen, Europhys. Lett. **94**, 27008(2011).

[19] F. Grønvold, H. Haraldsen, and J. Vihovde, Acta Chem. Scand. (1974-1973)**8**, 1927(1954).

[20] D. Fruchart, P. Convert, P. Wolfers, R. Madar, J. P. Senateur, and R. Fruchart, Mater. Res. Bull. **10**, 169(1975).

[21] H. Katsuraki and N. Achiwa, J. Phys. Soc. Jpn. **21**, 2238(1966).

[22] C. de la Cruz, Q. Huang, J. W. Lynn, J. Li, W. Ratcliff, J. L. Zarestky, H. A. Mook, G. F. Chen, J. L. Luo, N. L.Wang, and P. C. Dai, Nature **453**, 899 (2008).

[23] Q. Huang, Y. Qiu, W. Bao, M. A. Green, J. W. Lynn, Y. C. Gasparovic, T. Wu, G. Wu, and X. H. Chen, Phys. Rev. Lett. **101**, 257003 (2008).

[24] W. Bao, Y. Qiu, Q. Huang, M.A. Green, P. Zajdel, M.R. Fitzsimmons, M. Zhernenkov, M. Fang, B. Qian, E.K. Vehstedt, J. Yang, H.M. Pham, L. Spinu, and Z. Q. Mao, Phys. Rev. Lett. **102**, 247001 (2009).

[25] S. L. Li, C. de la Cruz, Q. Huang, Y. Chen, J. W. Lynn, J. P. Hu, Y. L. Huang, F. C. Hsu, K. W. Yeh, M. K. Wu, and P. C. Dai, Phys. Rev. B **79**, 054503(2009).

[26] L. J. Zhang, D. J. Singh, and M. H. Du, Phys. Rev. B**79**, 012506(2009).

[27] T. J. Liu, X. Ke, B. Qian, J. Hu, D. Fobes, E. K. Vehstedt, H. Pham, J. H. Yang, M. H. Fang, L. Spinu, P. Schiffer, Y. Liu, and Z. Q. Mao, Phys. Rev. B **80**, 174509(2009).

[28] M. E. Badding, J. Li, F. J. Disalvo, W. Zhou, and P. P. Edwards, J. Solid State Chem. **100**, 313-324(1992).

[29] S. X. Liu, G. L. Cai, and J. L. Huang, Acta Cryst. C **49**, 4-7 (1993).

[30] C. Pérez Vicente, M. Womes, J. C. Jumas, L. Sánchez, and J. L. Tirado, J. Phys. Chem. B **102**, 8712-8718(1998)

[31] J. L. Huang, Science in China, **43**, 337-347(2000).

[32] N. Nagaosa, J. Sinova, S. Onoda, A. H. MacDonald, and N. P. Ong, Rev. Mod. Phys. **82**, 1539(2010).

[33] J. G. Checkelsky, Minhyea Lee, E. Morosan, R. J. Cava, and N. P. Ong, Phys. Rev. B **77**, 014433(2008).

[34] C. G. Zeng, Y. G. Yao, Q. Niu, and H. H. Weitering, Phys. Rev. Lett. **96**, 037204(2006).

[35] E. Fawcett, Rev. Mod. Phys. **60**, 209 (1988).

[36] G. Grüner, Rev. Mod. Phys.**66**, 1-24 (1994).

[37] G. Grüner: Density waves in solids, Addison-Wesley, 1994